CRYSTAL GROWTH & DESIGN

Article

pubs.acs.org/crystal

Reversible Solid-State Hydration/Dehydration of Paroxetine HBr Hemihydrate: Structural and Thermochemical Studies

Paulo S. Carvalho, Jr.,[†] Cristiane C. de Melo,[†,‡] Alejandro P. Ayala,[‡] Cecilia C. P. da Silva,[†] and Javier Ellena*[,†]

[†]Instituto de Física de São Carlos, Universidade de São Paulo, CP 369, 13560-970 São Carlos, SP, Brazil

[‡]Departamento de Física, Universidade Federal do Ceará, CP 6030, Fortaleza, Ceará 60455-970, Brazil

Supporting Information

ABSTRACT: For active pharmaceutical ingredients (API) in the solid state, the occurrence of hydration/dehydration phase transitions may have implications upon the efficiency of the pharmaceutical product, once they are often accompanied by changes of physicochemical properties. Thus, it is important for pharmaceutical research and development to investigate these mechanisms based on the crystal structures of the API. In this work, beyond the structural characterization of a new salt of the antidepressant drug Paroxetine [an HBr hemihydrate, $(PRX^{+}Br^{-})\cdot 0.5H_2O$], by single crystal X-ray diffraction (SXRD), thermal analysis (DSC/TGA), and hot stage microscopy (HSM), we were able to perform a complete investigation toward the reversible hydration/dehydration solid phase transitions occurring for this salt. In addition, solubility measurements for the anhydrous and hemihydrate solid forms of the new salt are compared with those of its isostructural hydrochloride hemihydrate salt, $(PRX^{+}Cl^{-})\cdot 0.5H_2O$, for which hydration/dehydration processes are still not completely understood due to structure instability after dehydration.

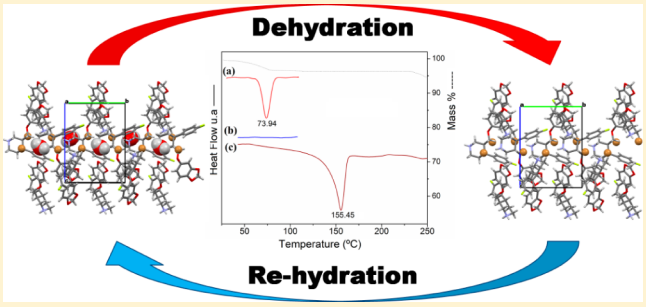

1. INTRODUCTION

Hydrates constitute the most physically stable form of an active pharmaceutical ingredient (API) under conditions of relative humidity (RH).[1−4] In the pharmaceutical context, it has been estimated that about one-third of API's are able to form hydrated structures[5] wherein the water is incorporated, stoichiometrically or nonstoichiometrically, in the crystal lattice. An important aspect of these compounds is the possibility of hydrate/dehydrate transformations induced by environmental changes. During manufacturing and storage steps, the drug product is exposed to a range of temperatures and water vapor pressures where the interaction between API and the water makes this ordinary phase transition possible.[2−4,6−9] Therefore, for practical and regulatory reasons, the search for the dehydrated phase(s) and the dehydration pathway are crucial to the development of a pharmaceutical product.[3,8,10−12]

Dehydration is a complex phenomenon that can involve the formation of multiples solid forms. The removal of water from the hydrated lattice may result in three possible scenarios: (*a*) an anhydrous solid form, generated by collapse of lattice; (*b*) an isomorphic/isostructural dehydrate, generated by the retention of the molecular packing of the parent hydrate; or (*c*) the complete alteration of lattice packing. Despite the systematic contributions to the mechanisms of solid state dehydrations, the topic remains a challenge, mainly due to the nonobvious relationship between hydrate/anhydrous lattices and the reversibility of the process. Also relevant, the lack of theses information can cause serious intellectual property (IP) issues in the end-use of a compound, as illustrated by a number of striking examples, such as the Paroxetine HCl case.[13,14]

Paroxetine (PRX) (Scheme 1) is an important antidepressant agent, widely used in the treatment of depression, panic, and obsessive-compulsive disorders, posttraumatic stress, and general anxiety.[15−23] Paroxetine HCl, the clinically utilized form of this API, can exist as a nonstoichiometric hydrate

Scheme 1. Chemical Structure of Charged Paroxetine (PRX^{+}) with the Numbering of Non-Hydrogen Atoms[a]

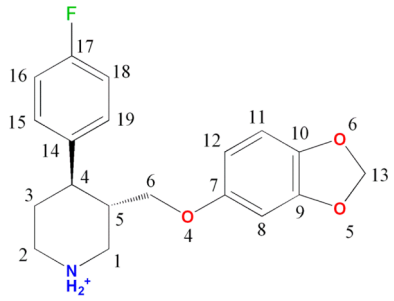

[a]The numerical atoms denomination for the two distinct conformers differ by adding the indices (′).

Received: November 25, 2015
Revised: January 22, 2016
Published: January 28, 2016

DOI: 10.1021/acs.cgd.5b01672
Cryst. Growth Des. 2016, 16, 1543−1549

(Form II), or as a hemihydrate (Form I, $(PRX^+Cl^-)\cdot 0.5H_2O$). In the last decades, efforts to protect PRX's patent from generic competition led to a big IP issue.[13,14,24,25] The production of the anhydrate from the $(PRX^+Cl^-)\cdot 0.5H_2O$ phase without the unknown conversion of anhydrous into hemihydrate was the core of patent litigations. The dehydration/rehydration process is complex, and even with concentrated efforts, it was difficult to control the presence of hemihydrate in the anhydrous product. Recent studies[26] have identified different anhydrous phases from the dehydration of Paroxetine HCl. Upon heating, Forms I and II give rise, respectively, to an anhydrous[14] and an isomorphic dehydrate.[26] The reversibility of each dehydration process was observed at low relative humidity conditions.[26]

In this study, with the aim of extending the solid state knowledge about PRX, we have rationalized the stability of Paroxetine HBr hemihydrate, $(PRX^+Br^-)\cdot 0.5H_2O$, with respect to its hydration/dehydration phenomenon. From a more fundamental point of view, the comparison between the isostructural $(PRX^+Cl^-)\cdot 0.5H_2O$ and $(PRX^+Br^-)\cdot 0.5H_2O$ salts have provided important features about relative stability among those phases. Finally, insights concerning the mechanism of the hydration/dehydration processes occurring for PRX could be completely provided for the first time, at the best of our knowledge, by combining structural information, molecular packing analysis, and direct observations of crystalline properties based on Differential Scanning Calorimetric (DSC), Thermogravimetric analysis (TGA), Hot−Stage Microscopy (HSM) and Variable temperature Single-Crystal X-ray diffraction (VT−SC−XRD) experiments. It is worth mentioning that this complete description was still not reported for the parent $(PRX^+Cl^-)\cdot 0.5H_2O$ salt, due its crystalline instability after dehydration, thus hindering the complete understanding of its spontaneous dehydration/rehydration mechanism.

2. EXPERIMENTAL DETAILS

Paroxetine HCl was obtained from commercial sources and used without any further purification. The sample consisted of Form I (Hemihydrate), as determined by powder X-ray diffraction (PXRD) pattern[27,28] and DSC analysis.[14,29] Organic solvents (analytical or spectroscopic grade) were also purchased from commercial sources and used as received.

2.1. Supramolecular Synthesis of Paroxetine HBr. In order to be able of synthesizing the proposed new salt, the first step was the achievement of PRX free base. For this, $(PRX^+Cl^-)\cdot 0.5H_2O$ (Form I) was used as the starting material, being dissolved in water, treated with excess of sodium hydroxide, and followed by gradual addition of ethyl ether. The mixture was then stirred until two phases became clear. The organic phase was separated from the water fraction and the ethyl ether phase was dried over Na_2SO_4. After removal of hydrated Na_2SO_4 by filtration, the evaporation of ethyl ether resulted in the oily free base of PRX. In sequence, 15 mg (0.045 mmol) of PRX free base was dissolved in 2 mL of ethanol 95%. After dissolution, 150 μL of HBr (1 mol·L^{-1}) were added to the system. The mixture was left to stand at −2 °C to allow for slow evaporation of the solvent. Colorless crystals appeared within a few days.

2.2. Single Crystal Determination Measurements. The crystallographic data for the $(PRX^+Br^-)\cdot 0.5H_2O$ were collected on a Bruker Super-Duo APEX II CCD diffractometer[30] using MoKα radiation (0.71073 Å). X-ray diffraction data collection for the PRX^+Br^- dehydrate was performed on an Enraf-Nonius Kappa-CCD diffractometer (95 mm CCD camera on κ-goniostat) using graphite-monochromated MoKα radiation (0.71073 Å) and an Oxford Cryo Systems *CryoStream 700Plus* to control the temperature. Using the Olex2[31] software, the structures were solved by direct methods and the models obtained were refined by full−matrix least-squares on F^2 (SHELXTL−97[32]). All the hydrogen atoms were placed in calculated positions and refined with fixed individual displacement parameters [$U_{iso}(H) = 1.2U_{eq}$ or $1.5U_{eq}$] according to the riding model (C−H bond lengths of 0.97 Å and 0.96 Å, for methylene and methyl groups, respectively). Molecular representations, tables and pictures were generated by Olex2,[31] MERCURY 3.2[33] and Crystal Explorer v2.1[34] programs.

The CIFs files of the $(PRX^+Br^-)\cdot 0.5H_2O$ collected at −173 °C, dehydrated at 87 °C and rehydrated at 25 °C were deposited in the Cambridge Structural Data Base[35] under the codes CCDC 1436946, CCDC 1436947, CCDC 1436953, respectively. Copies of the data can be obtained, free of charge, via www.ccdc.cam.ac.uk.

2.3. Thermal Analysis. Thermogravimetric analyses were carried out on a Shimadzu TGA-60 thermobalance. Approximately 3.5 mg of sample were placed on an alumina pan and heated from room temperature up to 200 °C, at 10 °C min^{-1}, under nitrogen flow (50 mL min^{-1}). Differential Scanning Calorimetric measurements were performed on a Shimadzu DSC-60 instrument. Samples (3.5 ± 0.5 mg) were aluminum pans and heated from room temperature up to 296 °C, at 10 °C min^{-1}, under nitrogen flow (50 mL min^{-1}). All data were processed using the Shimadzu TA-60 thermal data analysis software.

2.4. Hot-Stage Polarized Optical Microscopy. Microscopy was performed on a Leica DM2500P microscope connected to the Linkam T95-PE hot-stage equipment. Data were visualized with the Linksys 32 software for hot stage control. $(PRX^+Br^-)\cdot 0.5H_2O$ crystals were placed on a 13 mm glass coverslip, placed on a 22 mm diameter pure silver heating block inside of the stage. The sample was heated at a ramp rate of 10 °C min^{-1} up to a final temperature of 200 °C and interrupted after the melting of material.

2.5. Fourier Transform Infrared Spectroscopy (FTIR). FTIR spectra were recorded on a PerkinElmer Paragon 1000 spectrometer using KBr disks. Each spectrum was an average of 64 scans from 4000 to 400 cm^{-1} at 2 cm^{-1} of resolution. The spectrum of a blank KBr disk was used for the background correction.

2.6. DFT Calculations. Considering the presence of two conformer of PRX^+ (A and B) in the asymmetric unit of $(PRX^+Br^-)\cdot 0.5H_2O$, the electronic structure of A and B conformers of $(PRX^+Br^-)\cdot 0.5H_2O$ asymmetric unit was investigated within Density Functional Theory (DFT).[36,37] Starting from the X-ray structure the hydrogen position optimization was carried out using the 6-311++g(d,p) basis set and, M062X functional.[38] This functional was chosen due to its well-established performance for both hydrogen bonds and dispersion interactions. The zero-point vibrational energy (ZPVE) contributions ($E(A)_{ZPVE}$ and $E(B)_{ZPVE}$) were not neglected and energy difference (ΔE) between the conformers was calculated according to equation: $\Delta E = [E(A) + E(A)_{ZPVE}] - [E(B) + E(B)_{ZPVE}]$ where ($E + E_{ZPVE}$) represent the sum of electronic and zero-point Energies. All calculations were performed using Gaussian 09[39] suite program.

2.7. Solubility. Aqueous solubility was measured in distilled−deionized water by the flask saturation method.[40] The saturated solution of $(PRX^+Br^-)\cdot 0.5H_2O$ and $(PRX^+Cl^-)\cdot 0.5H_2O$ was prepared stirring a predetermined excess quantity (30 mg) of drugs in 400 μL of water for 24 h allowing to reach the thermodynamic equilibrium at 20 and 37 °C. After 4 h of sedimentation, the solution was filtered through a 0.45 mm filter (Millipore). The concentration of supernatant was measured by UV spectroscopy. Samples were then diluted 100-fold in water before analysis. The specific absorptivity was determined in distilled water, at the selected wavelength of λ_{max} = 293 nm and the standard solutions used to generate the calibration curve were prepared using $(PRX^+Cl^-)\cdot 0.5H_2O$. The concentration of the compound in the filtrate was quantified by interpolating of spectroscopic measurements from the diluted solutions in a calibration curve whose concentrations ranged from 0.005 to 0.2 mg. mL^{-1}. The solubility of PRXBr was determined in 2-propanol at 20 °C follow similar procedure.

DOI: 10.1021/acs.cgd.5b01672
Cryst. Growth Des. 2016, 16, 1543−1549

Table 1. Crystal Data and Structure Refinement of $(PRX^+Br^-)\cdot H_2O$ and (PRX^+Br^-)

	$(PRX^+Br^-)\cdot 0.5H_2O$	PRX^+Br^-
Empirical formula	$C_{38}H_{44}Br_2F_2N_2O_7$	$C_{19}H_{21}BrFNO_3$
Formula weight	838.57	410.28
Temperature/K	100(2)	360(2)
Crystal system	Monoclinic	Monoclinic
Space group	$P2_1$	$P2_1$
a/Å	12.9368(4)	12.9190(19)
b/Å	10.3393(4)	10.4970(10)
c/Å	14.3259(4)	14.5580(3)
β/°	107.464(2)	109.871(7)
Volume/Å^3	1827.87(11)	1856.7(5)
Z, Z′	4, 2	4, 2
ρ_{calc} (g/cm^3)	1.524	1.468
μ/mm^{-1}	2.280	2.241
F(000)	860.0	840.0
Crystal size/mm^3	0.083 × 0.05 × 0.044	0.083 × 0.277 × 0.543
Radiation	Mo Kα (λ = 0.71073)	Mo Kα (λ = 0.71073)
2θ range for data collection/°	3.724 to 51.628	5.96 to 49.86
Index ranges	$-15 \le h \le 15$, $-12 \le k \le 12$, $-17 \le l \le 17$	$-15 \le h \le 15$, $-12 \le k \le 11$, $-17 \le l \le 17$
Reflections collected	30984	14094
Independent reflections	6893 [R_{int} = 0.0632, R_{sigma} = 0.0712]	6222 [R_{int} = 0.094, R_{sigma} = 0.05]
Data/restraints/parameters	6893/1/472	6222/1/461
Goodness-of-fit on F^2	1.027	1.012
Final R indexes [I $\ge 2\sigma$ (I)]	R_1 = 0.0370, wR_2 = 0.0715	R1 = 0.0597, wR2 = 0.1498
Final R indexes [all data]	R_1 = 0.0477, wR_2 = 0.0747	R1 = 0.0903, wR2 = 0.1723
Largest diff. peak/hole/(e Å^{-3})	0.35/−0.41	0.28/−0.44
Flack parameter	0.008(5)	−0.0071(2)

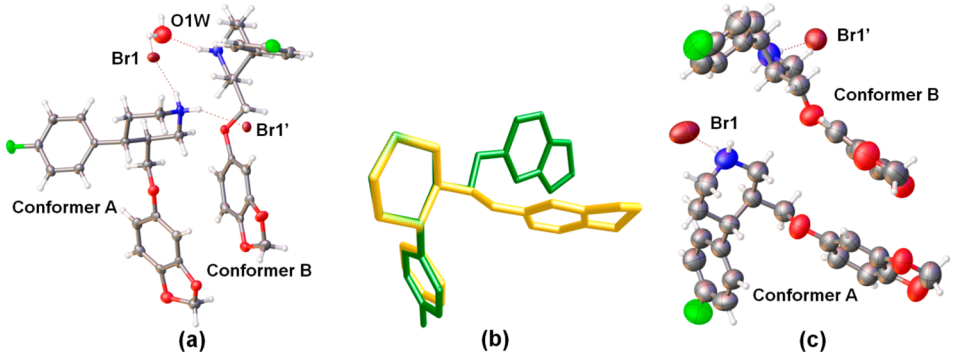

Figure 1. (a) Asymmetric unit of $(PRX^+Br^-)\cdot 0.5H_2O$. The ellipsoids were drawn at 30% of probability, the disorder occurring in the molecules H_2O and Br1 was omitted for clarity, and dashed red lines refer to the $N^+-H\cdots Br^-$ and $N^+-H\cdots Ow$ charge assisted H-bonds. (b) Overlap diagram of A-PRX^+ (green) and B-PRX^+ (yellow) conformers at their solid-state geometries, as determined by the diffraction experiment at T = −173 °C. The hydrogen atoms were hidden for clarity. The main conformational discrepancies are related with the C6−O4−C7−C8 torsion angle. (c) Asymmetric unit of (PRX^+Br^-). The ellipsoids were drawn at 30% of probability, the disorder occurring in the Br1 anion was omitted for clarity, and dashed red lines refer to the $N^+-H\cdots Br^-$ charge assisted H-bonds.

3. RESULTS AND DISCUSSION

3.1. Structural Description. A detailed description of the $(PRX^+Br^-)\cdot 0.5H_2O$ and (PRX^+Br^-) structures is depicted below. Table 1 exhibits the crystallographic data for the structures. The main intermolecular interactions for each salt are listed in Table S1 (Supporting Information). In Figure 1, a view of the asymmetric unit of each salt is shown.

Paroxetine HBr Hemihydrate Salt. The $(PRX^+Br^-)\cdot 0.5H_2O$ was successfully prepared by considering the similarity between the bromide and chloride anions. The salt was obtained by the simple acid−base reaction between the PRX free base and the HBr acid. The $(PRX^+Br^-)\cdot 0.5H_2O$ crystallizes in the monoclinic Sohncke space group $P2_1$ with two protonated PRX^+ molecules (A and B), two Br^- anions, and one crystallization water molecule in the asymmetric unit, exhibiting Z′ = 2 (Figure 1a). The A and B molecules constitute different conformations of PRX^+. Therefore, two nonequivalent PRX^+Br^- ionic pairs are present in the crystal structure, with one of the Br^- anions and the water molecule disordered. The PRX^+ molecular skeleton is dominated by σ-bonds. Then, this compound has a significant conformational flexibility that leads to conformational differences between conformers A and B. Figure 1b shows the main differences between the PRX^+ conformers, which were superimposed through their piperidinium moieties. The conformers differ by the orientation of the C6−O1−C7−C8 torsion angle [A: −147.4(4)° and B: −40.8(7)°, respectively]. Moreover, the five-membered 1,3-dioxolane rings (ring C) adopt different envelope conforma-

DOI: 10.1021/acs.cgd.5b01672
Cryst. Growth Des. 2016, 16, 1543−1549

tions with puckering coordinates[41] Q(2)A = 0.4196, ϕ(2)A = −46.90° for the A backbone and Q(2)B = 0.5103, ϕ(2)B = −44.91° for the B one. Nevertheless, both conformers are very close in terms of energy, with the B being more stable than the A conformation by just 2.41 kcal·mol^{-1} at the M062X/6-311++g(d,p) theory level.

PRX$^+$ lacks strong H-Bond donor functions, in a fashion that just two possible N$^+$−H hydrogen bond donors are available, belonging to the NH_2^+ group (Scheme 1), and is involved in charge assisted H-bonds (CAHB) of the types N$^+$−H···Br$^-$ and N$^+$−H···O (Figure 1a). As could be observed, in the crystal packing of (PRX$^+$Br$^-$)·0.5H_2O the water molecules play a key role in the formation of the main motifs between the PRX$^+$ conformers and the Br$^-$ anions, acting as ionic pair connectors. Along the [010] direction, a one-dimensional supramolecular $C_3^5(10)$ motif (highlighted in Figure 2) is formed between the

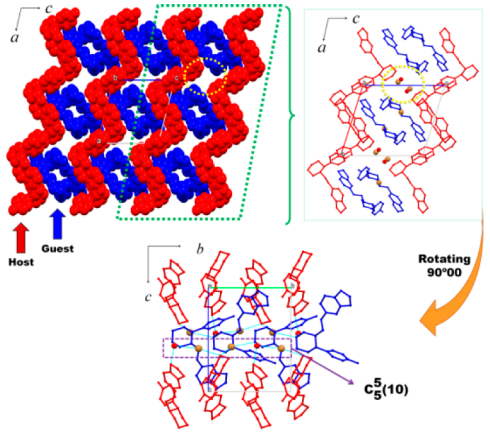

Figure 2. Perspective view of the PRX$^+$ framework along the *b*-axis showing the channels along the structure (highlighted in yellow circles), where the H_2O molecules and the Br$^-$ anions are hosted. Symmetry independent molecules of A host (blue) and B conformer guest (red) arrays in the crystal. Two distinct hydrogen bonded networks in the crystal structure of (PRX$^+$Br$^-$)·0.5H_2O.

Ow1 and both independent ionic pairs. In the same direction, symmetric $C_3^5(10)$ motifs merge into each other forming a $R_6^6(12)$ motif, leading to a complex infinite 2D-layer of molecules. This arrangement orientation of the conformers such as the drug framework can be understood as a host−guest complex, where "host" and "guest" molecules refer to PRX$^+$ conformers A and B, respectively (Figure 2). In this way, the host molecules are H-bonded to Br$^-$ and water molecules, forming zigzag chains (red in Figure 2), while the guest molecules are H-bonded only to Br$^-$, resulting in a square suprastructure (blue in Figure 2). The guest−host contacts are made by nonclassical C8−H8···π, C1−H1B···O2′, and C13−H13B···π intermolecular interactions (see Table 1S in the Supporting Information). In addition, the water molecules and Br$^-$ anions are located in circular channels running along the *b*-axis (highlighted in yellow in Figure 2).

Paroxetine HBr. The anhydrous PRX$^+$Br$^-$ crystalline phase (Figure 1c) was identified at 87 °C and is an isomorphic dehydrate (monoclinic Sohncke space group $P2_1$, Z′ = 2) of its parent hydrated form, (PRX$^+$Br$^-$)·0.5H_2O. In this way, similar volume and unit cell parameters are observed between both salts, being the differences smaller than 1.55% (Table 1). Also interesting is that even after dehydration no significant conformational changes on the PRX$^+$ molecules are observed. From a structural point of view, however, the dehydration requires a significant rearrangement of the main hydrogen bonds (see Figure S1 in the Supporting Information), in a fashion that the two strong N−H···Ow and O_w−H···Br hydrogen bonds observed in the (PRX$^+$Br$^-$)·0.5H_2O are replaced by NH_2^+···Br$^-$ hydrogen bonds in the anhydrous phase (Figure 1c). Nevertheless, it is worth noting that the radius of the circular channels, now composed only by Br$^-$ anions, remains unchanged.

3.2. Solid State Dehydration/Hydration Processes for Paroxetine HBr Hemihydrate. As depicted earlier, the dehydrated form of (PRX$^+$Br$^-$)·0.5H_2O is obtained at 87 °C. In this way, DSC, TGA and HSM measurements were carefully carried out aiming to understand the thermal behavior of (PRX$^+$·Br$^-$)·H_2O during these dehydration/hydration processes. The curve of the first heating DSC cycle (Figure 3a)

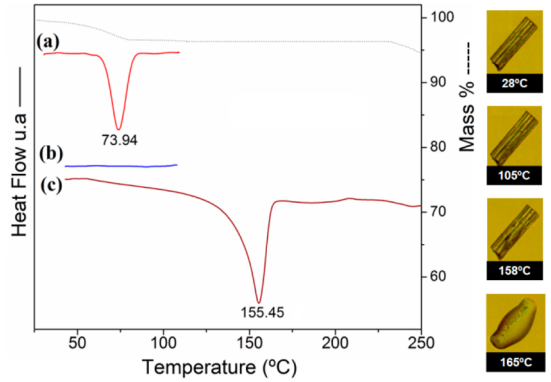

Figure 3. Heat−cool−reheat DSC curves (lines (a), (b), and (c), respectively), TGA (dashed gray line), and HSM for (PRX$^+$Br$^-$)·0.5H_2O, showing the crystal formation of the isomorphic dehydrate.

presents an endothermic peak in the temperature range of 50−80 °C and can be assigned as the dehydration process, once the TGA curve (Figure 3a) is accompanied by a small mass decrease in this same region, which agrees quite well with the release of water molecules from the crystal structure. Since the DSC cell is a closed system under nitrogen purge gas, no equivalent peak is observed during the cooling process (Figure 3b). However, a second endothermic peak is observed at 155 °C during the reheating process of the same sample (Figure 3c). This peak can be assigned as the melting of the resultant dehydrated material. In addition, it can be observed in the HSM experiment (right side of Figure 3) that at 158 °C the crystal starts to melt, changing its morphology, and that above 165 °C it has completely melted into a liquid droplet. Notoriously, the complete dehydration of (PRX$^+$·Br$^-$)·H_2O is not associated with any amorphization of the sample, neither change of habit or color before fusion. Also, according to the TGA data, after water loss the next event occurs only between 232 and 300 °C and is related with the thermal decomposition of the sample.

Based on the thermal analysis, a VT−SC−XRD experiment have been performed for (PRX$^+$Br$^-$)·H_2O, in a fashion that the dehydrated crystalline phase, identified at 87 °C, can be measured and the structure solved. Knowing that the porous channels present in the structure of PRX$^+$Br$^-$ (see section 3.1) can be readily accessible by water molecules, the consequent rehydration can be possible. In this way, if true, the reincorporation of water molecules in the solid state should give back the hydrated crystalline state, (PRX$^+$Br$^-$)·0.5H_2O.

DOI: 10.1021/acs.cgd.5b01672
Cryst. Growth Des. 2016, 16, 1543−1549

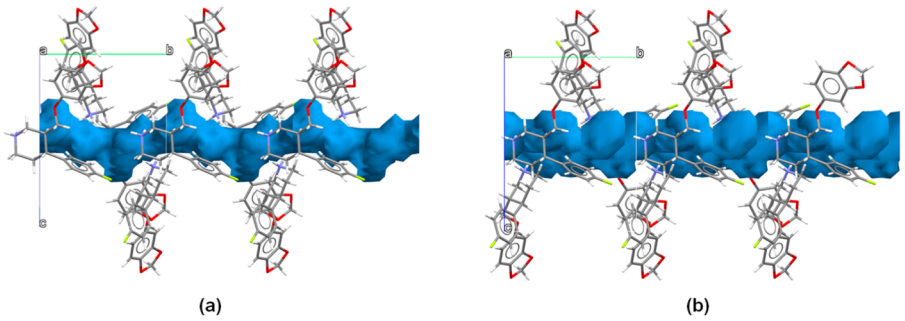

Figure 4. Crystal structure of (a) $(PRX^+Cl^-)\cdot 0.5H_2O$ and (b) $(PRX^+Br^-)\cdot 0.5H_2O$ hemihydrates with the water-containing channels highlighted in blue.

Thus, to state the reversibility of the dehydration of $(PRX^+Br^-)\cdot 0.5H_2O$ in the solid-state, the following protocol was adopted: (a) original crystalline samples were subjected to oven at 90 °C for 4h to get complete dehydration; (b) X-ray diffraction experiments of the dehydrated single crystals were performed to ensure complete dehydration at 87 °C; (c) the dehydrated crystalline samples were exposed to humid atmosphere for 2h; (d) the samples were measured by SXRD at 25 °C and DSC in order to confirm rehydration.

3.3. Comparison and Phases Relationship between $(PRX^+Br^-)\cdot 0.5H_2O$ and $(PRX^+Cl^-)\cdot 0.5H_2O$ Structures. Apart from similarity between chloride and bromide anions, it is interesting to note that the $(PRX^+Br^-)\cdot 0.5H_2O$ and $(PRX^+Cl^-)\cdot 0.5H_2O$[27,28] salts are isostructurals (see Hirshfeld discussion in the Supporting Information). In the Mercury 3.6,[33] a 20 PRX^+ molecules overlay (see Figure S2 in the Supporting Information) confirmed a high packing similarity between these crystal structures, having 20 out of 20 PRX^+ cations in common (RMSD = 0.204279 Å, 20% geometry tolerance and ignoring the smallest molecular component). This similarity suggests that the resultant motif formed by interactions of the type $N^+-H\cdots X$ (X = Cl, Br) is robust enough to mask the disturbances caused by electronegativity change, when Cl^- is replaced by Br^-.[42,43] In fact, a search of the Cambridge Structural Database[35] (Version 5.36 + updates), have shown that this is a very common supramolecular motif, not only occurring for Cl^- or Br^- anions, but also for others pairs of $N^+-H\cdots X$ CAHB involving protonated amide···halide (X = F^-, Cl^-, Br^-, I^-): a total of 4002 hits with 58.7% of them exhibiting chain motif, such as observed in the isostructural salts.

Differently from the $(PRX^+\cdot Br^-)\cdot H_2O$, no evident dehydration peak is observed in the DSC curve of $(PRX^+Cl^-)\cdot 0.5H_2O$ (see Figure S3 in the Supporting Information). The water loss in the HBr Form is detected in a large range of temperatures.[14,26,29] Despite the isostructurality, the thermal behavior differences between both salts suggest a dissimilar dehydration mechanism resulting in similar isomorphic dehydrates. However, dehydrated lattices from bromide and chloride hydrates differ in stability. The $(PRX^+Cl^-)\cdot 0.5H_2O$ salt have the lowest melting point, whereas the $(PRX^+\cdot Br^-)\cdot H_2O$ have the highest melting point. This observation agrees with the assumption that the CAHB $N^+-H\cdots Y$ (Y = Br^- or Cl^-) in the dehydrated lattice in both hemihydrates is stronger in the $(PRX^+Br^-)\cdot 0.5H_2O$ than in $(PRX^+Cl^-)\cdot 0.5H_2O$. In addition, the HCl salt degrades at a higher temperature relative to the HBr Form. This difference can result from the high reactivity of the bromide anion in the melting medium. Then, the $(PRX^+Cl^-)\cdot 0.5H_2O$ is more thermally stable than $(PRX^+\cdot Br^-)\cdot H_2O$.

As shown by Pina and coauthors,[14,26] the complex dehydration of the $(PRX^+Cl^-)\cdot 0.5H_2O$ occurs in a completely dry environment, RH ∼ 1%, at high temperatures, ∼75−100 °C. The resultant dehydrated phase is unstable and shows high affinity for water, which results in the fast spontaneous rehydration. For this reason, the detection of the event is not clearly evident, such as observed for the $(PRX^+Br^-)\cdot 0.5H_2O$. This supports the idea that changing the chloride by bromide results in slight structural differences that turn the dehydrate state more stable in the $(PRX^+Br^-)\cdot 0.5H_2O$ than in the $(PRX^+Cl^-)\cdot 0.5H_2O$. Although no crystal structure has been elucidated from the dehydration of $(PRX^+Cl^-)\cdot 0.5H_2O$ until now, similar conclusions can be inferred to this compound, by considering the packing similarity between both salts. Notwithstanding, the different rehydration mechanism for the PRX^+Br^- and PRX^+Cl^- dehydrates should be related to their respective structural features. After dehydration, it is impossible to fully satisfy the acceptor capacity of bromide ions (see Figure S1 in the Supporting Information). The replacement of water interactions by the Br^- in the PRX^+Br^- lattice induces steric strains resulting in a chemically unstable isomorphic system. Indeed, the channel structure is a fundamental feature to dehydration/rehydration behavior of both chloride and bromide salts. The channel structure of dehydrates allows the reincorporation of water without large structural rearrangement. However, the difference in the topology of the channels where the rehydration is preceded has a great impact in their phenomena kinetics. Because the bromide has the higher ionic radio than chloride, the channels in $(PRX^+Br^-)\cdot 0.5H_2O$ are twice as larger as in the $(PRX^+Cl^-)\cdot 0.5H_2O$. In addition, as shown in Figure 4, the spatial topography of channels in the HCl Form differ from the HBr by the presence of curvatures near y = 1/2 and y = 1. On one hand, the linear and more voluminous geometry of the channels in the $(PRX^+Br^-)\cdot 0.5H_2O$ facilitates the outflow of water in the dehydration, and in the other hand it also contributes to reducing the destabilizing effects in dehydrate structure when compared to the $(PRX^+Cl^-)\cdot 0.5H_2O$. As a result, while the rehydration of chloride occurs at ∼1 h, 75 °C at RH < 1%,[26] the rehydration of bromide was only observed at 2h, 25 °C at RH ∼ 75% (see Figure S4 in the Supporting Information).

3.4. Fourier Transform Infrared Spectroscopy. The structural similarities between $(PRX^+Br^-)\cdot 0.5H_2O$, $(PRX^+Cl^-)\cdot 0.5H_2O$ can also be inferred from their infrared spectra. The FTIR spectrum of $(PRX^+Br^-)\cdot 0.5H_2O$ (Form I) is shown in Figure 5. The FTIR spectrum of Form II (the dehydrated HBr

DOI: 10.1021/acs.cgd.5b01672
Cryst. Growth Des. 2016, 16, 1543−1549

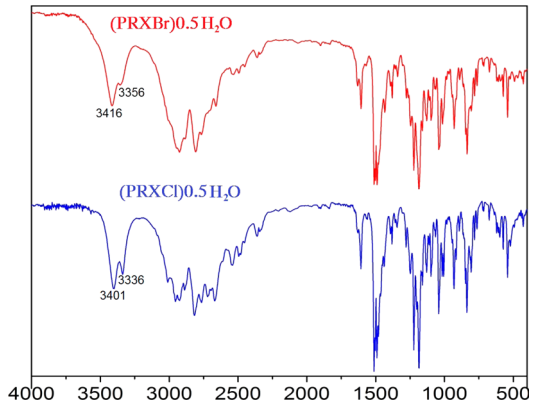

Figure 5. FTIR spectrum of the isostructural salts (PRXBr)·0.5H_2O and (PRXCl)·0.5H_2O, showing the stretching bands of the NH^{2+} group.

Form) was identical to Form I, and is thus omitted. In an attempt to establish a comparison, the FTIR spectrum of (PRX^+Cl^-)·0.5H_2O is also shown in Figure 5. The similarity in the molecular packing of these two isostructural salts is reflected on the similarity of their FTIR spectrum. For both salts, the main spectral features of the protonated PRX^+ molecule, such as the N−H stretching modes, could be easily identified. In fact, the amine group is used as fingerprint due its participation in strong hydrogen bonds. Primary amines are known to give rise to two NH stretching bands in the region of 3500−3300 cm^{-1}, and another band between 1650 and 1560 cm^{-1} due to the NH deformation mode. Stretching modes for the NH_2^+ group are seen at 3416 and 3356 cm^{-1} for (PRXBr)·0.5H_2O and at 3401 and 3336 cm^{-1} for (PRXCl)·0.5H_2O. Since the amine groups are particularly involved in hydrogen bonds with the counterion in both salts this considerable shift to higher frequencies in (PRXBr)·0.5H_2O is attributed to the decreasing electronegativity difference between Cl^- and Br^-.

3.5. Solubility of (PRX^+Br^-)·0.5H_2O, (PRX^+Cl^-)·0.5H_2O, and PRX^+Br^-. Solubility, by definition, is the measure of the maximum amount of solute dissolved in a given volume of solvent at a specified temperature.[44−46] This property is typically related to the melting point, the enthalpy of fusion, and supramolecular features together with the crystal lattice energy. This correlation is not a simple exercise and there are no reliable general rules, especially for salts.[45] The water solubility of (PRX^+Br^-)·0.5H_2O at 20 and 37 °C has been determined from a saturated aqueous solution. Due to spontaneous rehydration, the solubility of the PRX^+Br^- dehydrate has been determined only in 2-propanol.

The aqueous solubility of the (PRX^+Br^-)·0.5H_2O increases with temperature. At 20 °C, the (PRX^+Br^-)·0.5H_2O solubility is 2.66 ± 0.015 and increases to 3.10 ± 0.018 $mg.mL^{-1}$ when the temperature reach 37 °C. This small difference (~0.44 $mg.mL^{-1}$) indicates the high stability of this solid form when compared with its isostructural (PRX^+Cl^-)·0.5H_2O salt (S = 6.890 ± 0.2 mg/mL at 20 °C). The (PRX^+Br^-)·0.5H_2O is more soluble in 2-propanol, with the values differing (S = 8.61 ± 0.01 at 20 °C), from those estimated in water. As expected, due to the instability generated by the water removal, the PRX^+Br^- dehydrate displays a higher solubility in this organic solvent (S = 15.62 ± 0.01 $mg·mL^{-1}$). The value is significantly higher than its hydrate parent in the same solvent, and the solubility difference between the hydrated and anhydrous forms is approximately twice. In this view, the stability order of the forms was estimated. The (PRX^+Br^-)·0.5H_2O is thermodynamically more stable than its PRX^+Br^- dehydrate and, hence, less soluble. This thermodynamic relationship is consistent with those obtained by DSC.

4. CONCLUSIONS

The structural and thermal investigation of Paroxetine HBr has been performed. The determination of the crystal structure of the anhydrous and hydrate paroxetine HBr shows that the hydrate is isostructural to the ($PRX^+·Cl^-$)·H_2O. Despite the packing similarity, both forms have different thermal properties, mainly involving the desolvation process. The ($PRX^+·Cl^-$)·H_2O hemihydrate does not present a structural desolvation process while the ($PRX^+·Br^-$)·H_2O loses water molecules above 87 °C and still remains crystalline. The phenomenon is endothermic and is associated with the supramolecular arrangement of the water in the cavity and the organization of the channel. A cooperative desolvation mechanism has been proposed, since structural information is maintained after the water loss. No significant changes are observed in the molecular conformation and the relative position of the paroxetine molecules during the dehydration process, which results in an isomorphic dehydrate solid form. The anhydrous structure exhibits an increased solubility, indicating the relative stability among both forms. This work also suggests that the spontaneous rehydration process of (PRX^+Br^-) is related to the following features: (*i*) higher conformational similarity between PRX^+ molecules in anhydrous and hydrated forms; (*ii*) the relative stability of both forms; (*iii*) the presence of channels in the structure in which the molecule of water is accommodated; (*vi*) the restoration of strong OH···Br hydrogen bonds broken during the desolvation process; (*vii*) the more stable and cohesive structure generated after the rehydration.

■ ASSOCIATED CONTENT

Supporting Information

The Supporting Information is available free of charge on the ACS Publications website at DOI: 10.1021/acs.cgd.5b01672.

Crystal data and structure refinement, fractional atomic coordinates and equivalent isotropic displacement parameters, anisotropic displacement parameters, bond lengths and angles, torsion angles , hydrogen atom coordinates and isotropic displacement parameters, and atomic occupancy for (PRX^+Br^-)·0.5H_2O and PRX^+Br^-, and Hirshfeld surface and fingerprint plots, plus additional complementary tables and figures (PDF)

Accession Codes

CCDC 1436946, 1436947, and 1436953 contain the supplementary crystallographic data for this paper. These data can be obtained free of charge via www.ccdc.cam.ac.uk/data_request/cif, or by emailing data_request@ccdc.cam.ac.uk, or by contacting The Cambridge Crystallographic Data Centre, 12, Union Road, Cambridge CB2 1EZ, UK; fax: +44 1223 336033.

■ AUTHOR INFORMATION

Corresponding Author

*E-mail address: javiere@ifsc.usp.br.

Notes

The authors declare no competing financial interest.

DOI: 10.1021/acs.cgd.5b01672
Cryst. Growth Des. 2016, 16, 1543−1549

■ ACKNOWLEDGMENTS

The authors would like to acknowledge Brazilian funding agencies FAPESP (P.S.C.-Jr. grant 12/05616-7), CAPES, and CNPq for financial support.

■ REFERENCES

(1) Infantes, L.; Fabian, L.; Motherwell, W. D. S. *CrystEngComm* **2007**, *9*, 65.
(2) Aakeroy, C. B.; Forbes, S.; Desper, J. *CrystEngComm* **2012**, *14*, 2435.
(3) Khankari, R. K.; Grant, D. J. W. *Thermochim. Acta* **1995**, *248*, 61.
(4) Giron, D.; Goldbronn, C.; Mutz, M.; Pfeffer, S.; Piechon, P.; Schwab, P. *J. Therm. Anal. Calorim.* **2002**, *68*, 453.
(5) Griesser, U. J. In *Polymorphism*; Wiley-VCH Verlag GmbH & Co. KGaA: 2006; p 211.
(6) Bauer, J.; Spanton, S.; Henry, R.; Quick, J.; Dziki, W.; Porter, W.; Morris, J. *Pharm. Res.* **2001**, *18*, 859.
(7) Brittain, H. G. *J. Pharm. Sci.* **2008**, *97*, 3611.
(8) Kobayashi, K.; Kimura, S.; Togawa, E.; Wada, M.; Kuga, S. *Carbohydr. Polym.* **2010**, *80*, 491.
(9) Koradia, V.; Fontelonga de Lemos, A. F.; Allesø, M.; Lopez de Diego, H.; Ringkjøbing-Elema, M.; Müllertz, A.; Rantanen, J. *J. Pharm. Sci.* **2011**, *100*, 2896.
(10) Malaj, L.; Censi, R.; Gashi, Z.; Di Martino, P. *Int. J. Pharm.* **2010**, *390*, 142.
(11) Zhang, G. G. Z.; Law, D.; Schmitt, E. A.; Qiu, Y. *Adv. Drug Delivery Rev.* **2004**, *56*, 371.
(12) Tian, F.; Qu, H.; Zimmermann, A.; Munk, T.; Jørgensen, A. C.; Rantanen, J. *J. Pharm. Pharmacol.* **2010**, *62*, 1534.
(13) Bernstein, J. In *Polymorphism*; Wiley-VCH Verlag GmbH & Co. KGaA: 2006; p 365.
(14) Pina, M. F.; Pinto, J. F.; Sousa, J. J.; Fábián, L.; Zhao, M.; Craig, D. Q. M. *Mol. Pharmaceutics* **2012**, *9*, 3515.
(15) Stein, D. J.; Versiani, M.; Hair, T.; Kumar, R. *Arch. Gen. Psychiatry* **2002**, *59*, 1111.
(16) Bourin, M.; Chue, P.; Guillon, Y. *CNS Drug Rev.* **2001**, *7*, 25.
(17) Thal, D. M.; Homan, K. T.; Chen, J.; Wu, E. K.; Hinkle, P. M.; Huang, Z. M.; Chuprun, J. K.; Song, J.; Gao, E.; Cheung, J. Y.; Sklar, L. A.; Koch, W. J.; Tesmer, J. J. G. *ACS Chem. Biol.* **2012**, *7*, 1830.
(18) Hiemke, C.; Härtter, S. *Pharmacol. Ther.* **2000**, *85*, 11.
(19) Tanrikut, C.; Feldman, A. S.; Altemus, M.; Paduch, D. A.; Schlegel, P. N. *Fertil. Steril.* **2010**, *94*, 1021.
(20) Bowen, P. D. *Geriatric Nursing* **2009**, *30*, 85.
(21) Goudie, A. J.; Dubicki, W.; Leathley, M. *J. Pharm. Pharmacol.* **1988**, *40*, 192.
(22) Keller, M. B. Paroxetine treatment of major depressive disorder. *Psychopharmacol Bull.* **2003**, *37* (Suppl 1), 42.
(23) Saxena, S.; Brody, A. L.; Ho, M. L.; et al. *Arch. Gen. Psychiatry* **2002**, *59*, 250.
(24) Bernstein, J. *Polymorphism in Molecular Crystals*; Clarendon Press: 2002.
(25) Hilfiker, R. *Polymorphism: In the Pharmaceutical Industry*; Wiley: 2006.
(26) Pina, M. F.; Zhao, M.; Pinto, J. F.; Sousa, J. J.; Frampton, C. S.; Diaz, V.; Suleiman, O.; Fábián, L.; Craig, D. Q. M. *Cryst. Growth Des.* **2014**, *14*, 3774.
(27) Ibers, J. *Acta Crystallogr., Sect. C: Cryst. Struct. Commun.* **1999**, *55*, 432.
(28) Yokota, M.; Hidehiro, Uekusa; Yuji, Ohashi *Bull. Chem. Soc. Jpn.* **1999**, *72*, 1731.
(29) Bruni, G.; Sartor, F.; Berbenni, V.; Milanese, C.; Maietta, M.; Franchi, D.; Marini, A. *J. Therm. Anal. Calorim.* **2012**, *108*, 381.
(30) APEX2; Madison, Wisconsin, USA, 2009.
(31) Dolomanov, O. V.; Bourhis, L. J.; Gildea, R. J.; Howard, J. A. K.; Puschmann, H. *J. Appl. Crystallogr.* **2009**, *42*, 339.
(32) Sheldrick, G. *Acta Crystallogr., Sect. A: Found. Crystallogr.* **2008**, *64*, 112.
(33) Macrae, C. F.; Edgington, P. R.; McCabe, P.; Pidcock, E.; Shields, G. P.; Taylor, R.; Towler, M.; van de Streek, J. *J. Appl. Crystallogr.* **2006**, *39*, 453.
(34) Wolff, S.; Grimwood, D.; McKinnon, J.; Jayatilaka, D.; Spackman, M. *Crystal Explore 2.1*. University of Western Australia, Perth, 2007.
(35) Allen, F. *Acta Crystallogr., Sect. B: Struct. Sci.* **2002**, *58*, 380.
(36) Hohenberg, P.; Kohn, W. *Phys. Rev.* **1964**, *136*, B864.
(37) Kohn, W.; Sham, L. J. *Phys. Rev.* **1965**, *140*, A1133.
(38) Zhao, Y.; Truhlar, D. G. *Theor. Chem. Acc.* **2008**, *120*, 215.
(39) Frisch, M. J.; Trucks, G. W.; Schlegel, H. B.; Scuseria, G. E.; Robb, M. A.; Cheeseman, J. R.; Scalmani, G.; Barone, V.; Mennucci, B.; Petersson, G. A.; Nakatsuji, H.; Caricato, M.; Li, X.; Hratchian, H. P.; Izmaylov, A. F.; Bloino, J.; Zheng, G.; Sonnenberg, J. L.; Hada, M.; Ehara, M.; Toyota, K.; Fukuda, R.; Hasegawa, J.; Ishida, M.; Nakajima, T.; Honda, Y.; Kitao, O.; Nakai, H.; Vreven, T.; Montgomery, J. A.; Peralta, J. E.; Ogliaro, F.; Bearpark, M.; Heyd, J. J.; Brothers, E.; Kudin, K. N.; Staroverov, V. N.; Kobayashi, R.; Normand, J.; Raghavachari, K.; Rendell, A.; Burant, J. C.; Iyengar, S. S.; Tomasi, J.; Cossi, M.; Rega, N.; Millam, J. M.; Klene, M.; Knox, J. E.; Cross, J. B.; Bakken, V.; Adamo, C.; Jaramillo, J.; Gomperts, R.; Stratmann, R. E.; Yazyev, O.; Austin, A. J.; Cammi, R.; Pomelli, C.; Ochterski, J. W.; Martin, R. L.; Morokuma, K.; Zakrzewski, V. G.; Voth, G. A.; Salvador, P.; Dannenberg, J. J.; Dapprich, S.; Daniels, A. D.; Farkas; Foresman, J. B.; Ortiz, J. V.; Cioslowski, J.; Fox, D. J. *Gaussian*; Wallingford, CT, 2009.
(40) Eirkson, C. H. M., Osbourne, C. M., Sayre, P. G., Zeeman, M In *Environmental assessment technical assistance handbook*; U.S.F.D.A.: Washington, DC, 1987; Vol. *31*, p 1.
(41) Cremer, D.; Pople, J. A. *J. Am. Chem. Soc.* **1975**, *97*, 1354.
(42) Kalman, A.; Argay, G.; Scharfenberg-Pfeiffer, D.; Hohne, E.; Ribar, B. *Acta Crystallogr., Sect. B: Struct. Sci.* **1991**, *47*, 68.
(43) Haynes, D. A.; Jones, W.; Motherwell, W. D. S. *J. Pharm. Sci.* **2005**, *94*, 2111.
(44) Bhattachar, S. N.; Deschenes, L. A.; Wesley, J. A. *Drug Discovery Today* **2006**, *11*, 1012.
(45) Black, S. N.; Collier, E. A.; Davey, R. J.; Roberts, R. J. *J. Pharm. Sci.* **2007**, *96*, 1053.
(46) Cassens, J.; Prudic, A.; Ruether, F.; Sadowski, G. *Ind. Eng. Chem. Res.* **2013**, *52*, 2721.

DOI: 10.1021/acs.cgd.5b01672
Cryst. Growth Des. 2016, 16, 1543−1549